Wang, Dongchen; Tassi, Pablo

Secondary Flow Corrections into The Telemac-Mascaret Modelling System

Secondary Flow Corrections into The Telemac-Mascaret Modelling System

Dongchen Wang
Saint-Venant Hydraulics Laboratory (LHSV)
EDF R&D
Chatou, France

Pablo Tassi
Saint-Venant Hydraulics Laboratory (LHSV)
EDF R&D
Chatou, France
pablo.tassi@edf.fr

***Abstract*—In this work, the streamwise secondary correction model for the hydrodynamics field by Bernard and Schneider [3] is introduced. Hydrodynamics and morphodynamics results are presented and discussed on the basis of a selected number of test cases. Discussions on how secondary flow processes affect the estimation of the rate and the direction of sediment transport are given.**

I. PRELIMINARIES

Meandering rivers are ubiquitous in nature. In consequence, many human-related activities are closely related with their behaviour. At a river reach scale, the flow, the sediment transport and eventually the bank erosion in curved channels are of interest to the engineer who is in charge of maintaining navigation or to the designing of protection works. Following Schumm [11], channel pattern meandering can growth and shift creating major channel problems, as the flow reshapes the bend and bank erosion may become very serious.

In a curved channel, the flow experiences a radial acceleration and the centrifugal forces acts in proportion to the mean velocity. In turn, the surface of the water is tilted radially on the outer bank to produce a ``super-elevation" sufficient to create a pressure gradient to balance the average centrifugal force. At shallower depths, the centrifugal force exceeds the pressure force, whence the resultant force drives the fluid outwards. But deeper down the pressure force is the larger, causing the fluid to drift inwards [2]. In consequence, this imbalance produces a cross-stream component of the flow. Combined with downstream flow pattern, this induces the secondary (or helical, spiral) flow pattern characteristic of meandering bends. Experimental and in-situ observations showed that meander evolution strongly depends on the bed deformation, which in turn, drives the erosion process at the channel banks. It is therefore important to estimate the behaviour of flow and bed patterns at a channel bend.

In the literature, the parameterization of secondary flows in depth-averaged models has been tackled from different approaches. One of the most well-known approach is based on theoretical considerations for predicting velocity redistribution in meandering rivers and consisted on simplifications of the equation of motion combined with a parameterization of the primary velocity distribution through the vertical axis (see e.g., Johannesson and Parker [7, 8], Rozovskii [10], etc.). These models give in general satisfactory results of flow distribution for small curvature and uniform width bends. Another approach is based on the solution of an empirical transport equation for streamwise vorticity that mimics the depth-averaged influence of secondary flows. This approach has been proposed by Bernard and Schneider [3] and has been used to evaluate developing and decaying processes in secondary flows in irregular channels with nonuniform depth and curvature.

In the context of river morphology of alluvial bends, a reliable description of the influence of secondary currents is indispensable for an accurate estimation of the rate and the direction of sediment transport. Since the 70's, several works has been proposed to describe the interaction between the bed topography with water flow and sediment transport, when accounting the influence of secondary flows. Most of these approaches are based on considering gravitational and drag forces acting in the transverse direction due to the secondary flow [5]. Struiksma *et al.* [12] studied the bed deformation in river bends by considering the results of experiments in curved laboratory flumes, using linear and non-linear models. Similarly, Struiksma and Crosato [13] considered the effect of the downslope gravity force acting on a grain moving along a sloping bed and accounted for the effect of the spiral motion on the estimation of the expression for the direction of the bed shear stress.

However, the influence of secondary flows on momentum transfer in the streamwise direction can be important for the estimation of the bed shear stress, particularly for strongly curved bends. To the best of the authors' knowledge, few works have tackled the analysis of the influence of both secondary circulation effects in the streamwise and crosswise directions. Abad *et al.* [1] proposed a numerical tool to predict morphodynamics processes based on the existing hydrodynamics model STREMR. In their work, the correction for secondary flow effects in the hydrodynamics is done with the approach proposed by Bernard and Schneider [3] as well as corrections for secondary flows and bed transverse slope on sediment transport direction are funded respectively on the works of Engelund [5] and Koch and Flockstra [9].

The rate of change of the alluvial bed is in general solved via the solution of a continuity equation for the sediment. The morphological model therefore described as a function of the local gradient of the sediment fluxes, which in turn are function of the magnitude and direction of sediment transport models.

In the case of flows in a bend, the depth-averaged velocity is not a good parameter to describe the forces acting on the bed, since the helical secondary flow can be increase the bed shear stress component normal to the flow direction whilst their depth-averaged value equals to zero. In the literature, the formulation of the transport direction models is generally expressed as:

$$\delta = \delta^* - \Delta\delta \quad (1)$$

where δ^* is the direction of the bed shear stress and $\Delta\delta$ is the deviation of the bed shear stress relative to the streamlines, caused by the helical secondary flow. This angle can be determined as presented in Figure 1, where $\tau_{mainflow}$ is shear stress by the primary flow, $\tau_{\sec_s}$ is streamwise shear stress by secondary flow calculated by model of Bernard and Schneider [3], $\tau_{\sec_n}$ is transversal shear stress by secondary flow calculated by model of Engelund, τ_{sec} is shear stress with influence of secondary flow lift, G is gravity force from bed slope effect and τ_{real} presents the resultant direction of shear stress.

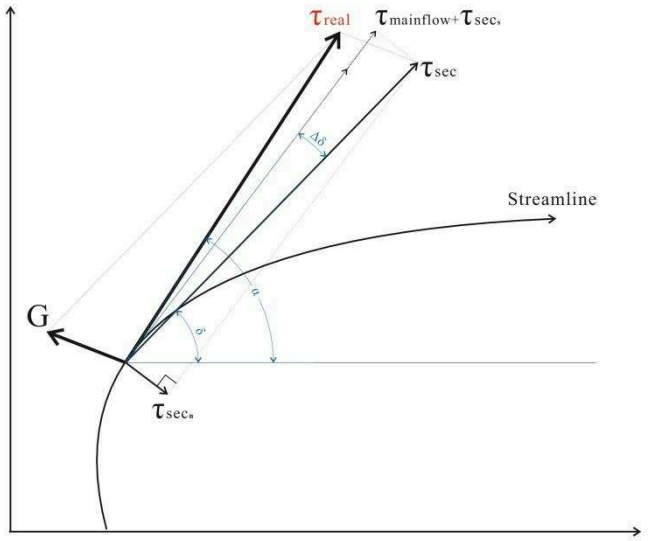

Figure 1. Forces acting on a sediment particle.

The objective of this work is therefore: (i) to introduce the streamwise secondary correction model for the hydrodynamics field proposed by Bernard and Schneider [3]; (ii) to describe and clarify some important aspects of the crosswise correction of secondary flows proposed by Engelund [5] and to analyse how both processes affect the estimation of the rate and the direction of sediment transport; and (iii) to verify and validate these models with a selected number of test cases. Finally, a summary of new keywords and printout variables adapted to the Telemac-Mascaret is given in the Appendix.

II. CORRECTION FOR SECONDARY FLOW EFFECTS ON THE DEPTH-AVERAGED HYDRODYNAMICS FIELD

Bernard and Schneider [3] proposed a secondary flow correction for two-dimensional depth-averaged hydrodynamics models. The model parameterizes the usually neglected dispersion terms that arise from the depth-average form of the Navier-Stokes momentum equations.

The developing and decaying processes of secondary flows in curved channels can be accounted by solving the transport equation for streamwise vorticity, from which the shear stress associated with secondary flows is determined:

$$\frac{\partial \Omega}{\partial t} + \underbrace{u\frac{\partial \Omega}{\partial x} + v\frac{\partial \Omega}{\partial y}}_{vortex\ advection} = \underbrace{\frac{A_s\sqrt{C_f}|u|^2}{Rh\left(1+\frac{9h^2}{R^2}\right)}}_{vorticity\ production} - \underbrace{D_s\sqrt{C_f}\Omega\frac{|u|}{h}}_{vorticity\ dissipation} + \underbrace{\frac{1}{h}\nabla(\upsilon h\nabla\Omega)}_{vortex\ diffusion\ (turbulence)} \quad (2)$$

with Ω the streamwise vorticity, C_f is a friction coefficient, ν the eddy viscosity, R the local radius of curvature, and A_s, D_s empirical coefficients that determine the rate of vorticity production and dissipation, respectively. The solution of Equation (2) allows the calculation the streamwise stresses that result from the deviation of velocity from the depth-averaged velocity:

$$\tau_s = \rho h\,|\boldsymbol{u}|\Omega\sqrt{C_f} \quad (3)$$

where ρ is the water mass density.

In a Cartesian coordinate system, the accelerations induced by secondary currents are computed as follows:

$$\boldsymbol{S} = (S_x, S_y) \approx \rho^{-1}\frac{\boldsymbol{u}}{|\boldsymbol{u}|}\left[\boldsymbol{n}\cdot\nabla(h\tau_s) + \frac{2h\tau_s}{R}\right] \quad (4)$$

with h the water depth and $\boldsymbol{n}$ = unit vector normal to the depth-averaged velocity vector $\boldsymbol{u}$, with components (u, v) and module $|\boldsymbol{u}|$. In (4), the term $\boldsymbol{n}\cdot\nabla(h\tau_s)$ can be written as:

$$\boldsymbol{n}\cdot\nabla(h\tau_s) = \frac{v(h\tau_s)_x - u(h\tau_s)_y}{|\boldsymbol{u}|}$$

and the local radius of curvature determined by the expression:

$$R = \frac{|\boldsymbol{u}|^3}{uv(v_y - u_x) + u^2 v_x - v^2 u_x}. \quad (5)$$

In short, the solution steps needed to incorporate the secondary currents correction into the depth-averaged hydrodynamics field are summarized below:

- Solve the shallow water equations for velocity and depth **without** the secondary flow correction
- Solve transport equation for vorticity (2), with R computed from expression (5)
- With Ω, solve Eq. (4) to compute the accelerations $\boldsymbol{S} = (S_x, S_y)$ induced by secondary currents, with R computed from expression (5) and τ_s from (3)

- Plug the accelerations that result from the non-uniformity of the velocity field in the vertical direction $\boldsymbol{S} = (S_x, S_y)$into the shallow water equations and solve the SWE **with secondary flow correction**

III. CORRECTION FOR SECONDARY FLOW ON THE DIRECTION OF THE BED SHEAR STRESS

In curved channels, the direction of the sediment transport will no longer coincides with the direction of the bed shear stress due to the effect of the secondary flows. Engelund proposed a semi-empirical expression to incorporate this effect into depth-averaged models [5]. We refer to this as **crosswise vorticity** correction.

The bed shear stress in the main flow direction can be written as:

$$\tau^* = \frac{C_f}{2}\rho|\boldsymbol{u}|u \tag{6}$$

The bed shear stress for the transverse direction can be written as:

$$\tau^{\sec_n} = \tau^* \tan\Delta\delta, \tag{7}$$

with

$$\delta = \tan^{-1}\left(\frac{v}{u}\right) - \tan^{-1}\left(\frac{A}{R}h\right) = \delta^* - \Delta\delta. \tag{8}$$

The term $tan^{-1}\left(\frac{A}{R}h\right)$ indicated in Equation (8) accounts for the effect of the spiral motion on the sediment flux. The angles δ^* and $\Delta\delta$ indicate respectively the direction of the bed shear stress (which coincides with the direction of the depth-averaged velocity) and the direction due to the effect of secondary currents. The cos and sin of the angle δ^* can be computed by:

$$\cos\delta^* = \tau_x^*/|\boldsymbol{\tau}^*|, \qquad \sin\delta^* = \tau_y^*/|\boldsymbol{\tau}^*| \tag{9}$$

with τ_x^* and τ_y^* the components of the bed shear stress from the momentum equations related to the depth-averaged velocity field, with module $|\boldsymbol{\tau}^*| = \sqrt{(\tau_x^*)^2 + \left(\tau_y^*\right)^2}$.

Several expressions have been proposed for the spiral coefficient A. Engelund proposed a constant coefficient $A = 7$ and Struiksma *et al.* proposed:

$$A = \frac{2\epsilon}{\kappa^2}\left(1 - \frac{\sqrt{g}}{\kappa C}\right) \tag{10}$$

where ϵ is a calibration coefficient, $\kappa = 0.4$ is the von Karman constant and C is the Chézy friction coefficient.

For bends, the slope of the water surface can be approximated by:

$$g\frac{\partial z_s}{\partial n} \simeq \frac{\alpha'|\boldsymbol{u}|^2}{R}, \tag{11}$$

with z_s the water surface elevation and α' a coefficient accounting for rough or smooth beds, with $0.75 \le \alpha' \le 1.0$. The curvature radius can be then expressed by:

$$\mathrm{R} = \frac{\alpha'|\boldsymbol{u}|^2}{g\partial z_s/\partial n}. \tag{12}$$

The normal derivative of the water surface elevation can be calculated as:

$$\frac{\partial z_s}{\partial n} = \boldsymbol{n}\cdot\nabla \mathrm{z_s} = \frac{u\partial z_s/\partial y - v\partial z_s/\partial x}{|\boldsymbol{u}|} \tag{13}$$

By replacing Equation (13) into (12):

$$R = \frac{\alpha'|u|^3}{g(u\partial z_s/\partial y - v\partial z_s/\partial x)} \tag{14}$$

By using (7), the bed shear stress **due to secondary currents** is then given by:

$$\tau^{sec_n} = \frac{C_f}{2}\rho\frac{Ah}{\alpha'}g|\boldsymbol{u}|\frac{1}{R} \tag{15}$$

with components

$$\tau_x^{\sec_n} = \tau^{\sec_n} v,\ \tau_y^{\sec_n} = \tau^{\sec_n}(-u). \tag{16}$$

Finally, the components of the bed shear stress including the influence of secondary currents are:

$$\tau_x^{\sec} = \tau_x^* + \tau_x^{\sec_n},\ \tau_y^{\sec} = \tau_y^* + \tau_y^{\sec_n}. \tag{17}$$

with

$$\cos\delta = \tau_x^{\sec}/|\tau^{sec}|,\ \sin\delta = \tau_y^{\sec}/|\tau^{sec}|. \tag{18}$$

and $|\boldsymbol{\tau}^{\boldsymbol{sec}}| = \sqrt{\tau_x^{sec^2} + \tau_y^{sec^2}}$ the module of the bed shear stress, including the effect of secondary currents.

IV. CORRECTION FOR SECONDARY FLOW AND TRANSVERSE BED SLOPES DUE TO GRAVITY ON THE MORPHODYNAMICS

The total bedload can be decomposed into $x-$ and $y-$ direction components as

$$q_b = \left(q_{b_x}, q_{b_y}\right) = (q_b\cos\alpha\,, q_b\sin\alpha), \tag{19}$$

with q_b the bedload transport rate per unit width, computed as a function of the equilibrium sediment load closure q_{b_0}, see below and α the direction angle of bedload.

A larger group of equilibrium sediment load closures can be usually written as a function of the excess Shields stress $(\theta - \theta_c)$ for a given particle Reynolds number R_p :

$$q_{b_0} = f\left(\theta - \theta_c; R_p\right) \tag{20}$$

with bed shear stress θ and the critical Shields parameter θ_c. For example, the dimensionless form of the Meyer-Peter and Müeller expression is given by:

$$q_{b_0} = 8(\mu\theta - \theta_c)^{\frac{3}{2}} \quad (21)$$

where μ is the ripple coefficient.

Next, the expressions for the correction of the direction and intensity of the sediment transport by combined effect of secondary flows and bed slope are given.

A. Direction of the sediment transport

The angle α is the angle between the sediment transport direction and the $x-$ axis direction will deviate from that of the shear stress by combined action of a transverse slope and secondary currents:

$$\tan\alpha = \frac{\sin\delta - \frac{1}{f(\theta)}\frac{\partial z_b}{\partial y}}{\cos\delta - \frac{1}{f(\theta)}\frac{\partial z_b}{\partial x}} \quad (22)$$

Above, the terms $\partial z_b/\partial x$ and $\partial b/\partial y$ represent respectively the transverse and longitudinal slopes. The sediment shape function $f(\theta)$ is a function weighting the influence of the transverse bed slope, expressed as a function of the dimensionless shear stress or Shields parameter θ, computed as:

$$\theta = \frac{|\tau|}{(\rho_s - \rho)g d_{50}} \quad (23)$$

Several expressions have been proposed in the literature for $f(\theta)$, e.g. Koch and Flokstra $f(\theta) = 3\theta/2$; Talmon *et al.* $f(\theta) = \beta_2\sqrt{\theta}$, with the coefficient $0.35 \le \beta_2 \le 1.5$; and Struiksma *et al.*:

$$f(\theta) = 9\left(\frac{d_{50}}{h}\right)^{0.3}\sqrt{\theta} \quad (24)$$

B. Intensity of the sediment transport

The influence of bed slopes on the sediment transport rate (i.e. not on the direction) can be accounted by three different approaches:

1) The Struiksma and Crosato's approach: The intensity of the sediment transport rate is modified by a corrective term that accounts for the bed slope through the gradients of the bottom:

$$q_b = q_{b_0}\left(1 + \chi\frac{\partial z_b}{\partial s}\right)$$

$$= q_{b_0}\left(1 + \chi\left(\frac{\partial z_b}{\partial x}\cos\alpha + \frac{\partial z_b}{\partial y}\sin\alpha\right)\right) \quad (25)$$

where χ is a coefficient accounting for the streamwise bed slope effect. Struiksma and Crosato proposed $\chi = \epsilon C^2/g$, with C the Chezy's coefficient and ϵ a calibration coefficient ($\epsilon = \mathcal{O}(10^{-2})$).

2) The Soulsby approach: This approach suggests that the effect of bed slopes on the sediment transport rates is caused entirely by a change of the critical Shields parameter in the equilibrium sediment transport formula. In this case:

$$q_b = q_{b_0}(\theta - \theta_c'; R_p) \quad (26)$$

with θ_c' the modified critical Shields stress computed by the expression:

$$\theta_c' = \frac{\cos\delta\sin\beta + \sqrt{\cos^2\beta\tan^2\phi - \sin^2\delta\sin^2\beta}}{\tan\phi}\theta_c \quad (27)$$

with ϕ the angle of repose and $\beta$the angle to the horizontal.

V. Model Verification

To validate the present model, we simulated different cases well documented in the literature. For all simulations, a depth-averaged $k-\varepsilon$ model was used to parameterize the turbulence effects. For all simulations, the streamwise secondary flow correction coefficients were set to $A_s = 7$ and $D_s = 0.5$.

A. Hydrodynamics

1) The Riprap Test Facility: The secondary flow correction proposed by Bernard and Schneider [3, 6] has been tested on experimental data from the Riprap Test Facility conducted at the Waterway Experiment Station of the U.S. Army Engineer Waterways Experimental Station [3]. The channel presented four bends and two reversals in curvature, with $L = 274m$ long and $B = 3.63m$ wide with a bed slope of 2.16‰ and 2H:1V bank side slopes, see Figure 2. Numerical simulations were performed with a constant discharge $q_{in} = 4.25m^3/s$ at inlet and mean flow depth $h_{out} = 0.8m$ at outlet. The channel bed has been treated as rigid, with the friction coefficient C_f specified with the Manning relation with a roughness coefficient $n = 0.026\, s/m^{-1/3}$.

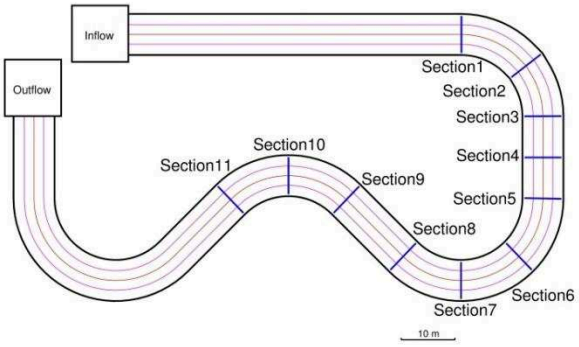

Figure 2. Geometry and cross-sections for the Riprap Test Facility.

The computational domain has been discretized with a non-structured triangular finite element mesh with a total of 25577 elements and 13340 nodes, with mean element size of $0.4m$. The discretization of the banks was done with 5 elements on

each side of the channel. The numerical experience was run for $\approx$ 4min until the equilibrium stage was reached, with a time step $\Delta t = 0.01s$. Numerical results of depth-averaged velocities were compared to measured velocities previously averaged throughout the water depth at cross-sections 1 to 11 indicated in Figure 2. The secondary flow correction coefficients were set to $A_s = 7$ and $D_s = 0.5$.

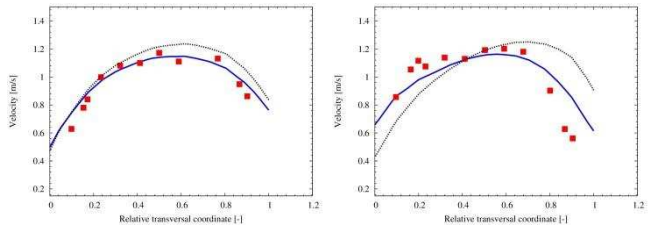

(a) section 1 (b) section 2

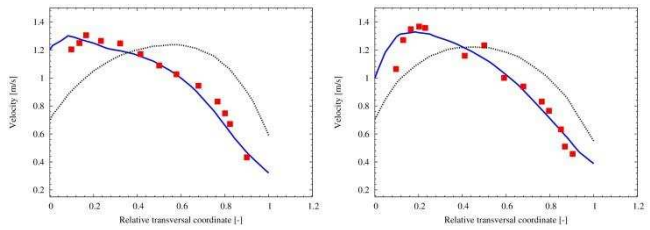

(c) section 3 (d) section 4

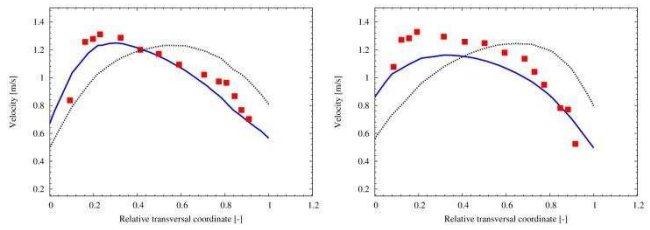

(e) section 5 (f) section 6

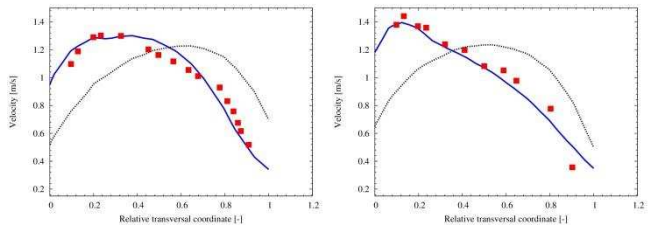

(g) section 7 (h) section 8

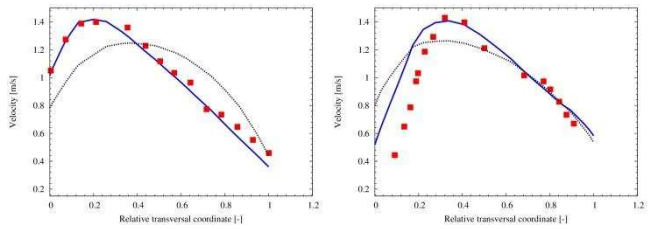

(i) section 9 (j) section 10

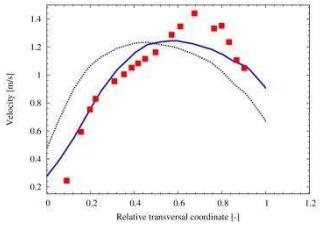

(k) section 11

Figure 3. Comparison of experimental (red dots) and numerical results computed with (solid blue lines) and without (dashed lines) the correction of secondary flows on the hydrodynamics for sections 1 to 11.

The simulated and measured depth-averaged velocities at the 11 individual cross-sections are shown in Figure 3. For each section, comparisons between observed and computed depth-averaged velocities with and without the secondary flow correction are given. For the different sections, the zero-distance on the transversal coordinate indicates the position of the left bank facing downstream. At section 1, the comparison of the flow distribution upstream of the first bend entrance is well reproduced by both the corrected and uncorrected models, showing a better match of the highest velocity prediction when the secondary flow correction is activated. For sections 2 to 5, the secondary flow correction improves dramatically the predicted results without secondary flow effects. In particular, for sections 3 to 5 the model reproduces very well the highest velocities located near the left boundary. For section 6, located upstream of the second bend, the corrected model captures well the shape of the flow distribution but underpredicts the values of the hightest velocities of about $0.2m/s$. In contrast, the uncorrected model fails to capture both the velocity distribution and velocity magnitudes. From sections 7 to 10, the corrected model predicts very well the maximum velocities that are shifted to the left bank. For section 11, the prediction using the corrector agrees the observed velocity distribution but underestimates the maximum velocity.

2) Channel Bend Facility test: Detailed velocity measurements conducted on a two-bends S-shaped flume at the Waterway Experiment Station have been used for further verification of the secondary flow corrector. The channel presented two 100° bends with a reversals in curvature, with $L = 34.78\,m$ long and $B = 2.134m$ wide with a bed slope of 2.5‰and 2H:1V bank side slopes, see Figure 4. Numerical simulations were performed with a constant flow rate at inlet $q_{in} = 0.191m^3/s$ at inlet and a mean water elevation $h_{out} = 0.139m$ at outlet. As for the previous test, the channel bed has been treated as rigid, with the friction coefficient C_f specified with the Manning relation with a roughness coefficient $n = 0.020\,s/m^{-1/3}$.

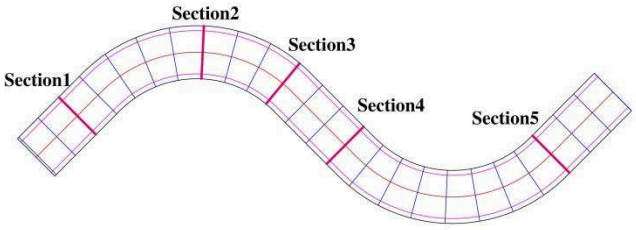

Figure 4. Geometry and cross-sections for the Channel Bend Facility test. The flow is from left to right.

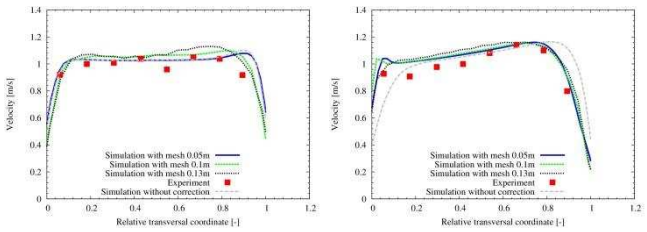

(a) section 1 (b) section 2

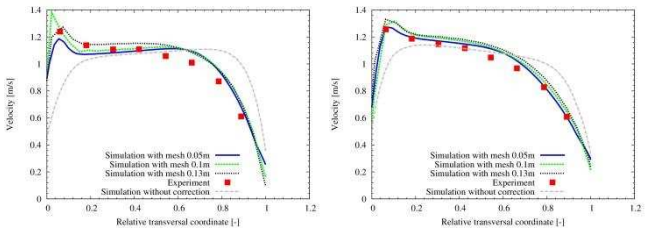

(c) section 3 (d) section 4

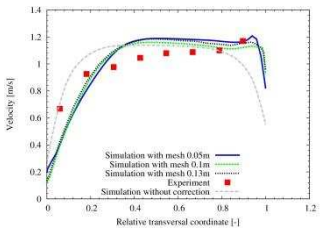

(e) section 5

Figure 5. Comparison of experimental and numerical results with and without secondary currents correction for sections 1 to 5.

The computational domain has been discretized with a non-structured triangular finite element mesh with a total of 78838 elements and 40259 nodes, with mean element size of $0.05m$. The discretization of the banks is with 5 elements. The numerical experience was run for $\approx$ 4min until the equilibrium stage was reached, with a time step $\Delta t = 0.01s$. Numerical results of depth-averaged velocities were compared to measured velocities previously averaged throughout the water depth at cross-sections 1 to 5 indicated in Figure 4. The secondary flow correction coefficients were set to $A_s = 7$ and $D_s = 0.5$. As before, comparisons between observed and computed depth-averaged velocities with and without the secondary flow correction are given for each section. The zero-distance on the transversal coordinate indicates the position of the left bank facing downstream.

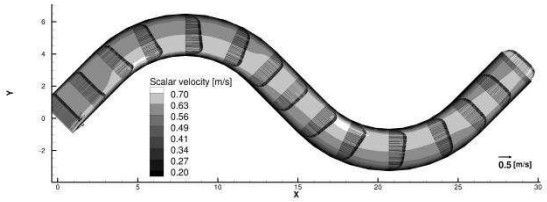

(a)

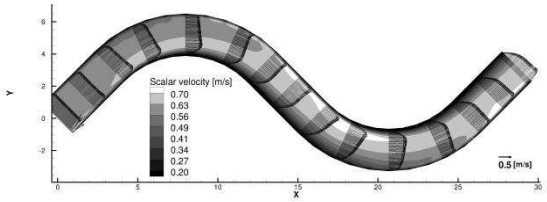

(b)

Figure 6. Comparison of numerical results with or without secondary currents correction, (a) simulation result without correction, (b) simulation result with correction.

Numerical simulations of depth-averaged velocities are in generally satisfactory agreement with observations when secondary flow corrector is incorporated into the hydrodynamics model, see Figure 5. Conversely, the uncorrected model is not able to reproduce some of the features of the flow that are typically observed in curved channels, such as velocity projected towards the left bank in Figures 5(c) and 5(d). At Section 5, some discrepancies between the measured and computed velocity distribution are observed, although the maximum velocity at the right bank is well captured by the corrected model.

Figure 5 depicts also a sensitivity analysis for a gradual mesh refinement, with typical mesh sizes of $0.15m$, $0.10m$ and $0.05m$. Although similar results are obtained with the different meshes, the finer mesh captures more accurately the sharper flow zones. Figure 6 shows contour plots of velocity module and depth-averaged velocity vectors for simulations with and without the correction of secondary flows on the hydrodynamics. A noticeable observed feature is that the magnitude of the velocity is increased in the region located on the left bank upstream of the second bend and thereafter projected toward the right bank at the channel outlet. This phenomena is in agreement with the experimental observations.

B. Morphodynamics

In the following sections, morphodynamics computations were performed assuming bedload transport with the Meyer-Peter & Müller sediment transport formula. Furthermore, lateral bed slope processes were incorporated with the Talmon expression, with $\beta_2 = 0.75$. Struiksma and Crosato's approach is used to correct the intensity of the sediment transport caused by bed slope effect. For each simulation case, different tests are made to test the influences of the streamwise (Bernard and Schneider [3] correction) and crosswise (Engelund [5] correction) secondary flow corrections. The streamwise secondary flow correction coefficients were set to $A_s = 7$ and

$D_s = 0.5$. Three-dimensional numerical simulations were used as reference results.

1) LFM Curved Flume: The experimental data from the Laboratory of Fluid Mechanics Curved Flume (LFM) were used to evaluate the capabilities of the model to reproduce the formation of a point bar and pool length in a $180-$deg bendway. The geometry of the flume agree with natural meander planforms. The experiences were conducted at the Delft University of Technology, The Netherlands on a curved flume with fixed banks with bend radius $R_c = 4.25m$, bend length $L_c = 13.35m$ and width $B = 1.7m$. The bed slope was $1.8‰$ and Chézy coefficient $C = 26.4m^{1/2}/s$. The flow rate at inlet was $q_{in} = 0.17m^3/s$ and water elevation at outlet was $h_{out} = 0.20m$. The sediment medium grain size was $d_{50} = 0.78mm$, with a Shields parameter $\theta = 0.28$. The planform of the channel is shown in the Figure 7(a). In Figure 7(b), the contours of the measured equilibrium bed topography are showed, characterized by the presence of a forced or point bar located upstream of the bend and a pool found at the outer concave bank (Figure reproduced from Koch and Flockstra [9]).

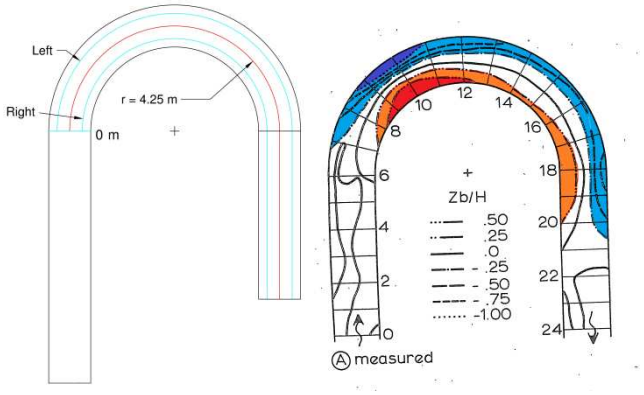

(a) (b)

Figure 7. LFM Curved Flume: (a) geometry and cross-sections; (b) measured equilibrium bed topography (reproduced from Koch and Flockstra [9]).

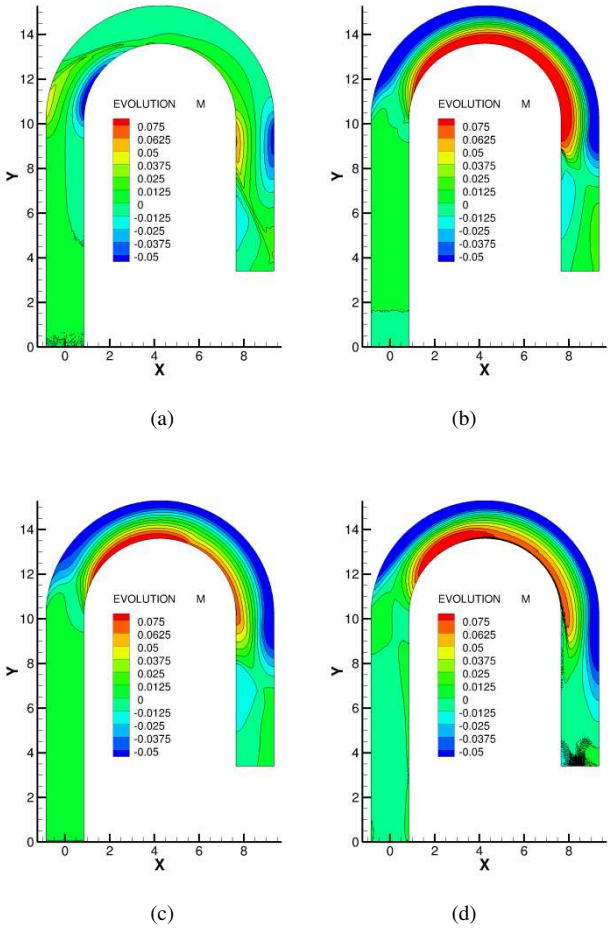

(a) (b)

(c) (d)

Figure 8. Comparisons of simulation results with and without secondary currents corrections, (a) Simulation without any corrections, (b) simulation with correction of Engelund, (c) simulation with correction of Bernard and Schneider [3] and Engelund [5], (d) 3D simulation result.

The bed topography depicted in Figure 8(a) has been obtained from a morphodynamics numerical simulation without any correction for accounting secondary flow effects. Clearly, the absence of a mechanism accounting for cross stream pressure gradients and centrifugal acceleration impedes the establishment of a velocity field and, in consequence, the development of a bed topography characteristic of curved channels.

Figure 8(b) presents the bed topography obtained from a morphodynamics numerical simulation that includes the cross-wise vorticity correction presented in §III. Although the results have been dramatically improved respect to the solution obtained with the model without correction, some differences arise from a visual comparison with observations. The position of the forced bar and pool is in accordance with the experimental observations but the bar dimensions do not seem to be similar to those observed in the experiments. Furthermore, the numerical simulation is not able to capture the first pool located approximately where the projection of the tangent to the inner bank intersects the outer bank.

Figure 8(c) shows the bed topography obtained from a morphodynamics numerical simulation that includes both the streamwise and the crosswise vorticity corrections presented in §II and §III, respectively. In accordance with observations, a pronounced point bar and pool configuration is developed upstream of the bend and well reproduced by the model. The numerical results are also in agreement with those obtained with a three-dimensional model.

VI. MODEL VALIDATION

The parameterization of the physical processes underlying in meandering rivers is addressed by reproducing the flow structures and bed deformation of the in-bank experiments carried out on the U.K. Flood Channel mobile bed testing Facility (FCF) at HR Wallingford. It consists of a $10m$ wide and $60m$ long tank within which a sine-generated meandering channel. The sinuosity $= 1.34$, cross over angle $\omega = 60°$ and wavelength $M = 14.96m$. The valley slope is $1.83‰$. The channel has a 1H:1V side bank slope in the straight part of channel, and has a vertical bank at the outer bank of the meandering bend apex. The water mixed with sediment flows in from left inlet of the channel< with a discharge constant of $q_{in} = 0.097m^3/s$, and downstream outlet is with fixed water depth of $h_{out} = 1.4335m$. Originally, the bed material had a $d_{16} = 0.35mm$, $d_{50} = 1.33mm$, and $d_{84} = 3.19mm$, these were adopted in the numerical experiences presented below.

The computational domain has been discretized with a non-structured triangular finite element mesh with a total of 62927 elements and 32442 nodes, with mean element size of $0.05m$. The lateral discretization of the banks is with 3 elements. The numerical experience was run for $\approx 10h$ until the equilibrium stage was reached, with a time step $\Delta t = 0.01s$. The secondary flow correction coefficients were set to $A_s = 7$ and $D_s = 0.5$. The channel bed has been treated as rigid, with the friction coefficient C_f specified with the Nikuradse relation with a roughness coefficient $k_s = 0.008m$.

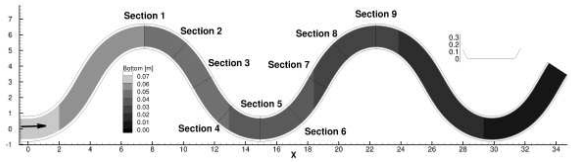

Figure 9. Geometry of test case FCF experiment.

A. Flow structures

Flow patterns computed with and without secondary flow corrections are presented in Figure 10. Clearly, the combined effect of Bernard and Schneider and Engelund correctors reproduce the secondary circulation around the channel bend that creates a pool around the outer bank, with sediment fluxes being transported from the outer to the inner bank, forming the point bar. This behaviour is typical of many natural channels, as identified by Dietrich [4].

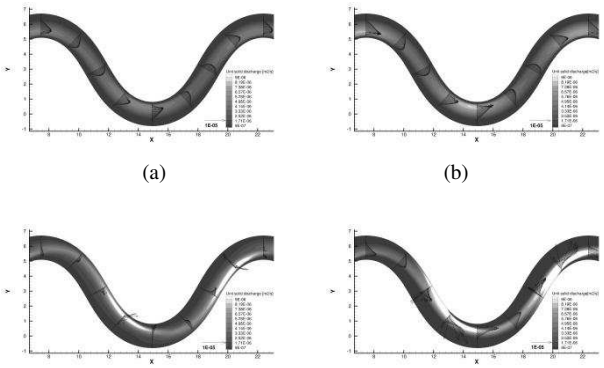

(a) (b) (c) (d)

Figure 10. Comparisons of direction of solid discharge with and without secondary currents corrections, (a) Simulation without any corrections, (b) simulation with correction of Engelund, (c) simulation with correction of Bernard and Schneider [3] and Engelund [5], (d) 3D simulation result.

B. Morphodynamics structures

A comparison of morphological characteristics obtained from simulations activating/deactivating secondary currents processes parameterizations is presented in Figs 11 (a, b and c), and compared with a sketch summarizing the main morphodynamics structures presented in the meandering flume in Figure 11(d). The line connecting the lowest bathymetric points follows the outer bank until it moves across the point bar just upstream of the bend apex toward the outside of the following bend.

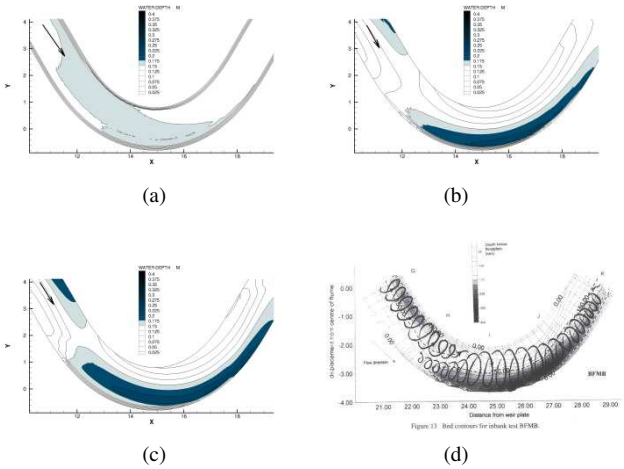

(a) (b) (c) (d)

Figure 11. Comparisons of simulation results with and without secondary currents corrections, (a) Simulation without any corrections, (b) Simulation with correction of Engelund, (c) Simulation with correction of Bernard and Schneider [3] and Engelund [5], (d) Observations [14].

VII. CONCLUSIONS

Secondary currents processes for the hydrodynamics field, based on Bernard and Schneider work [3], have been implemented for the release **v7.0** of the Telemac-Mascaret Modelling system. Numerical examples showed the importance of incorporating this corrector to incorporate the non-uniformity of the velocity field in the vertical direction into depth-averaged models. We also described and clarified some important aspects of the crosswise correction of

secondary flows proposed by Engelund [5] and analysed how their combined effects could affect the estimation of the rate and the direction of sediment transport and therefore on morphodynamics computations.

REFERENCES

[1] J. Abad, G. Buscaglia, and M.H. Garcia. 2d stream hydrodynamic, sediment transport and bed morphology model for engineering applications. Hydrological Processes, 22(10):1443–1459, 2008.

[2] J.R.L. Allen. Principles of Physical Sedimentology. George Allen & Unwin Ltd.,. London, Boston, Sydney, 1985.

[3] R. Bernard and M. Schneider. Depth-averaged numerical modeling for curved channels. Technical report, DTIC Document, 1992.

[4] W.E. Dietrich. Mechanics of flow and sediment transport in river bends. Richards, K. (ed.), River Channels Environment and Process. Blackwell, London, 1987.

[5] F. Engelund. Flow and bed topography in channel bends. Journal of the Hydraulics Division, 100(11):1631–1648, 1974.

[6] J. Finnie, B. Donnell, J. Letter, and R. Bernard. Secondary flow correction for depth-averaged flow calculations. Journal of Engineering Mechanics, 125(7):848–863, 1999.

[7] H. Johannesson and G. Parker. Secondary flow in mildly sinuous channel. Journal of Hydraulic Engineering, 115(3):289–308, 1989.

[8] H. Johannesson and G. Parker. Velocity redistribution in meandering rivers. Journal of hydraulic engineering, 115(8):1019–1039, 1989.

[9] F.G. Koch and C. Flokstra. Bed level computations for curved alluvial channels: prepared for the 19th IAHR-congress, New Delhi, India, Febr. 1981. Publication (Waterloopkundig Laboratorium (Delft, Netherlands))). Delft Hydraulics Lab., 1980.

[10] I. L. Rozovskii. Flow of water in bends of open channels. Academy of Sciences of the Ukrainian SSR, 1957.

[11] S.A. Schumm. Patterns of alluvial rivers. Annual Review of Earth and Planetary Sciences, 13:5, 1985.

[12] N. Struiksma, K.W. Olesen, C. Flokstra, and H.J De Vriend. Bed deformation in curved alluvial channels. Journal of Hydraulic Research, 23(1):57–79, 1985.

[13] N. Struiksma and A. Crosato. Analysis of a 2-D Bed Topography Model for Rivers. Wiley Online Library, 1989.

[14] P.R. Wormleaton, R.H.J. Sellin, T. Bryant, J.H. Loveless, R.D. Hey, and S.E. Catmur. Flow structures in a two-stage channel with a mobile bed. Journal of Hydraulic Research, 42(2):145–162, 2004.

APPENDIX

A summary of Telemac-2d new keywords and printout variables is given below.

A. *New keywords*

SECONDARY CURRENTS HYDRO: by default: NO.

COEFFICIENT OF PRODUCTION FOR SECONDARY CURRENTS: by default: 5.E0.

COEFFICIENT OF DISSIPATION FOR SECONDARY CURRENTS: by default: 5.E-1.

B. *Printout variables*

1/R: The reverse of local radius: $1/r_{\mathrm{sec}}$

OMEGA: Vorticity of the flow: Ω

TAU_S: Streamwise stresses: τ_s